JOURNAL OF SOLID STATE CHEMISTRY 43, 163–174 (1982)

Conductivities and Electronic Structures of Some Phases in the Lithium–Iron–Sulfur System*

S. P. S. BADWAL† AND R. J. THORN

Chemistry Division, Argonne National Laboratory, 9700 South Cass Avenue, Argonne, Illinois 60439

Received September 30, 1981; in revised form February 26, 1982

During the electromigration of lithium ions from molten LiCl–KCl mixtures into FeS three of the phases formed are Li_2FeS_2 (X phase), $Li_3Fe_2S_4$ (Z phase), and $LiK_6Fe_{24}S_{26}Cl$ (J phase). These phases and the copper-substituted X phase ($Li_{1.33}Cu_{0.67}FeS_2$) were prepared by high-temperature solid-state reactions between the respective metal sulfides, and their electrical conductivities were measured over temperatures ranging from 20 to 550°C. The results show that the X and copper-substituted X phases are semiconductors with conductivities and activation energies in the range of 0.1 to 10 $(ohm\text{-}cm)^{-1}$ and of 8 to 21 kJ $mole^{-1}$, respectively. The Z phase has a conductivity orders of magnitude less, and the J phase decomposes. A change in the slope of the Arrhenius plot occurs at 225°C, probably associated with some residue of the phase change in the FeS component. The electronic structures determined with photoelectron spectroscopy reveal the presence of two valence states for iron in the X, copper-substituted X, and Z phases. The valence bands consist of overlaping Fe(3*d*), Cu(3*d*), and S(3*p*) electronic densities.

Introduction

Several phases of various compositions have been observed in the Li–Fe–S system (*1*, *2*). Among these are two with the compositions corresponding to Li_2FeS_2 (*2–4*) and $Li_3Fe_2S_4$ (*5*), which form through the electromigration and displacement reaction of lithium ions in the FeS and FeS_2 phases. Recently, these phases have been found in the FeS and FeS_2 cathodes of the lithium–sulfur battery (*3–5*); consequently, their properties are needed to understand the solid-state chemistry of these cathodes. The rate of electrochemical reaction in the cathode is controlled by the chemical and electrical properties of the Li–Fe–S phases. The discharge and charge behaviors are complex in contrast to solid-solution electrode systems where the lithium ions diffuse into a host lattice which simply acts as a reservoir in which no new phases are formed. However, the advantage of these cathodes is that the discharge occurs at a constant voltage because of the presence of two phases. Knowledge of the electrical properties and electronic structures of the intermediate Li–Fe–S phases formed should contribute significantly toward a better understanding of the performance of the battery. To obtain some of the needed

* Work performed under the auspices of the Office of Basic Energy Sciences, Division of Chemical Sciences, U.S. Department of Energy, under Contract W-31-109-Eng-38.

† Present address: Advanced Materials Laboratory, Division of Materials Science, CSIRO, Box 4331, G.P.O., Melbourne, Victoria 3001, Australia.

0022-4596/82/080163-12$02.00/0

information, we prepared the two phases cited above and two related phases, $Li_{1.33}Cu_{0.67}FeS_2$ and $LiK_6Fe_{24}S_{26}Cl$, and we measured their conductivities and determined their photoelectron spectra.

Previously reported investigations of X-ray crystallographic structures and the Mössbauer spectra have been reported for some of the phases (*6, 7*). In the Li_2FeS_2 phase two positions for the iron are indicated, but the evidence for two valence states is obscure. The Li_2FeS_2 and copper-substituted phases are pseudohexagonal; the structure of the $Li_3Fe_2S_4$ phase is unknown; and the phase with the formula $LiK_6Fe_{24}S_{26}Cl$ has a structure which resembles djerfisherite.

Experimental Procedures

Sample Preparation

Li_2FeS_2 (X phase).[1] This phase was prepared by mixing the fine powders (particle size <40 μm) of Li_2S (99.9%) and FeS (99.999%) in equal molar proportions and reacting the resulting mixture first at 890 ± 10°C for 2 hr and then at 825 ± 5°C for 50–65 hr. The mixture was contained inside a tightly sealed graphite crucible, and an atmosphere of high-purity argon was maintained over it throughout the course of the experiment.

$Li_{1.33}Cu_{0.67}FeS_2$ (copper-substituted X phase). This phase was prepared in a similar fashion to X phase but by replacing 33% of Li_2S with Cu_2S. The reaction was initially carried out at 925 ± 5°C for 15 hr and then at 840 ± 5°C for 95 hr.

$Li_3Fe_2S_4$ (Z phase). Several attempts to prepare $Li_3Fe_2S_4$ from mixtures of FeS, Fe_2S_3, and Li_2S were unsuccessful. Finally this phase was prepared by heating a disk (pressed at a pressure of 200–250 MN-m^{-2}) of a mixture containing FeS, FeS_2, and Li_2S in the molar ratio 1.5 : 0.5 : 1.5 at 450°C for 140 hr, crushing the disk to a fine powder, repressing the resulting powder into another disk, and firing it at 450 ± 5°C for 95–100 hr. The second half of the procedure was repeated.

$LiK_6Fe_{24}S_{26}Cl$ (J phase). This phase was prepared by two methods:

(*i*) Li_2S and FeS were mixed in a 2 : 1 molar ratio and reacted with KCl and an Armco iron rod in molten LiCl–KCl at 440 ± 5°C for 100 hr. The reaction was carried out in an alumina crucible enclosed inside a graphite crucible. Excess of Li_2S and LiCl–KCl was removed by treating the resulting product with water. (All the components of the mixture except J phase are soluble in water.) The residue was washed several times with distilled water and ethanol. The product was dried under vacuum first at room temperature and then at ~50°C.

(*ii*) This method is similar to the one described above. Prepared Li_2FeS_2 phase was reacted with excess Li_2S and molten LiCl–KCl in an Armco iron crucible at 440 ± 5°C for 100 hr. The phase prepared by this method was more crystalline.

The prepared phases were examined by X-ray diffraction and metallographically. The X phase contained minor traces of the $Li_7Fe_2S_6$ (*4*) phase. Cu–X phase was free of contamination by other phases. For J phase, the X-ray pattern indicated only the presence of single phase but metallographic examination indicated the presence of a substantial amount of another phase. The Z phase contained 3–5% of an unknown phase. Chemical analysis performed on these phases is given in Table I. The sum of the percentage composition is less than one hundred by approximately 5%. This result is consistent with the analyses reported by Melandres and Tani (*7*). Since the material which did not dissolve during the analytical procedure was negligible compared with 5%, the discrepancy cannot be assigned to

[1] The designation of these phases is that used in the technological program in the Chemical Engineering Division at Argonne National Laboratory.

TABLE I

COMPOSITIONS OF THE Li–Fe–S PHASES

Phase		Composition			
		Lithium	Iron	Sulfur	Copper
Li_2FeS_2(X)	Exptl	9.6	40.4	45.7	—
	Calcd	10.4	41.7	47.9	—
$Li_{1.33}Cu_{0.67}FeS_2$	Exptl	4.6	31.7	34.8	?
	Calcd	5.4	32.5	37.3	24.8
$Li_3Fe_2S_4$	Exptl	7.3	40.9	46.4	—
	Calcd	8.0	42.8	49.2	—

insoluble material such as carbon. The most plausible source of the discrepancy is moisture which the sample absorbed after the samples were removed from the dry box for chemical analysis.

In order to prepare samples for conductivity measurements, the phases were crushed into a fine powder (particle size <40 μm) and pressed into cylindrical disks at a pressure of 200–250 MN-m^{-2}. The resulting disks were 6–10 mm long and 9.5 mm in diameter. They were sintered at higher temperatures. The details of the sintering conditions and the density of the disks are given in Table II. The end faces of the disks were filed flat and polished with 1200A silicon carbide paper.

Since most of these phases are moisture sensitive, the preparation, handling, and loading of the samples were done in a glovebox under high-purity argon atmosphere. The moisture content inside the glovebox was less than 3–5 ppm.

Conductivity Measurements

A four-probe dc conductivity technique was used for making measurements. For this purpose the four-probe conductivity cell shown in Fig. 1 was constructed. The current probes were constructed by painting flux-free platinum paste (Hanovia Liquid Gold 6926) on the polished ends of the disks and by drying the organic disperser by heating the sample at 50–60°C in vacuum. The procedure was repeated until a uniform and thick layer of platinum paste was obtained. Platinum foil current collectors were pressed onto each end, and the assembly, held between two alumina disks, was mounted in a stainless-steel clamp (Fig. 1b). Various components of the cell were kept together by applying compressive stress via a tungsten compression spring. Potential probes were constructed by grinding one end of a 1.9-mm-diameter tungsten rod to a fine tip. The probes were held a fixed distance apart with machineable glass components mounted in a stainless steel jig (Fig. 1c). The probes were lowered onto the sample with a hinged arrangement, and pressure to the probes was applied with tungsten compression springs as shown in Fig. 1d. The probe spacing was measured with a microscope equipped with a traveling stage and a micrometer. The conductiv-

TABLE II

SINTERING CONDITIONS FOR VARIOUS PHASES

	Li_2FeS_2(X)		$Li_{1.33}Cu_{0.67}FeS_2$(Cu–X)		$Li_3Fe_2S_4$(Z)		$LiK_6Fe_{24}S_{26}Cl$(J)
	Sample 1	Sample 2	Sample 1	Sample 2	Sample 1	Sample 2	Sample 1
Time (hr)	55	70	70	135	100	100	—
Temperature (°C)	780 ± 10	786 ± 10	810 ± 20	765 ± 10	450 ± 5	450 ± 5	—
Density[a] (g cm^{-3})	2.35	2.41	2.98	2.97	1.77	1.75	2.19

[a] X-Ray densities for these phases except J phase (3.66 g cm^{-3}) are not known.

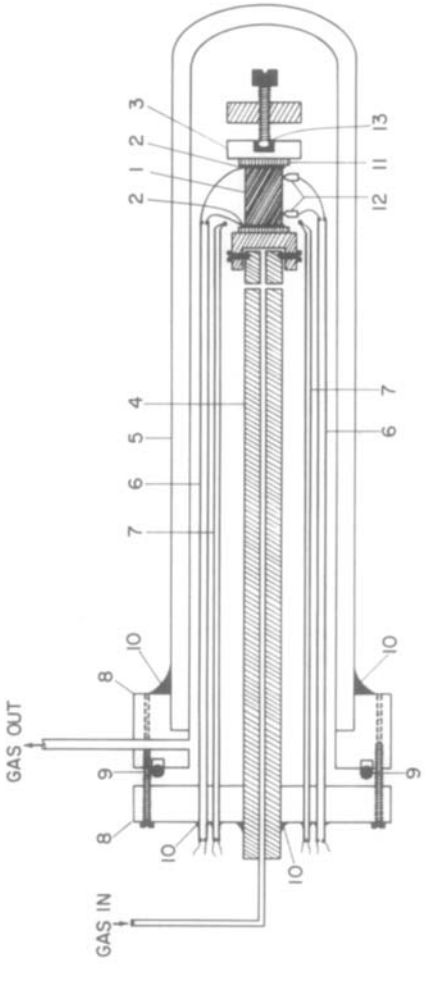

a

FIG. 1a. Four-probe conductivity apparatus. (1) Sample. (2) Platinum current probes. (3) Stainless-steel clamp for holding sample. (4) Stainless-steel rod with a bore in the center. (5) Quartz tube. (6) Twin-bore alumina tube. (7) Thermocouple. (8) Brass components. (9) O ring. (10) Epoxy. (11) Alumina insulators. (12) Potential probes (Fig. 1d). (13) Spring.

ity cell was enclosed inside a quartz tube through which argon gas was flushed continuously, and was purified by passing it through a furnace containing copper shot at 500°C and then through another furnace containing titanium at 900°C. Connections to the potential and current probes were made with platinum wires (0.015–0.030 in).

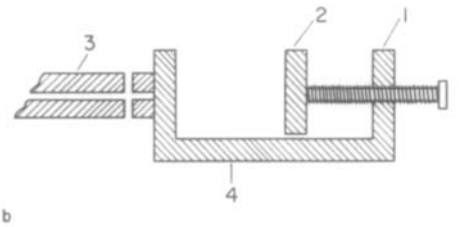

b

FIG. 1b. Stainless-steel clamp. (1) Stationary component of the clamp. (2) Moving plate. (3) Stainless-steel rod (4) in Fig. 1a. (4) Position for screwing potential probe clamp.

A gold mirror insulation furnace (Trans Tempo Co.) was used for heating the conductivity samples, and chromel–alumel and Pt–10%Rh/Pt thermocouples were used for temperature control and measurements. A Barber Coleman 560 series process controller and CB40 series power controller controlled the temperature of the furance to within ±1°C.

A constant current between 100 μA–10 mA was passed from a Keithley constant current source Model 227. The potential drop across the potential probes was measured directly with a Keithley Model 616 digital electrometer or a Dana Model 5500 digital voltmeter; alternatively the signal from the potential probes was preamplified

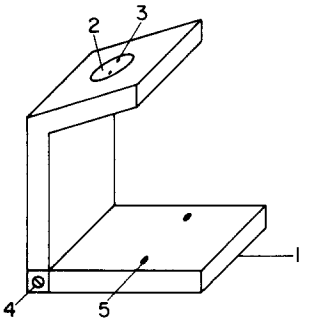

c

FIG. 1c. Potential probe clamp. (1) Stainless-steel plate that screws onto stainless-steel clamp at position 4 in Fig. 1b. (2) Machineable glass components (Fig. 1d). (3) Tungsten potential probes. (4) Hinge. (5) Screw holes.

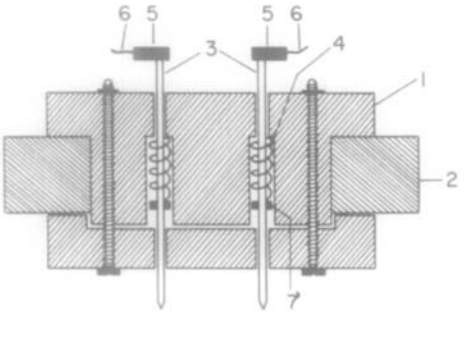

FIG. 1d. Detailed potential probe arrangement. (1) Machineable glass component. (2) Stainless-steel plate. (3) Tungsten potential probes. (4) Tungsten springs. (5) Stainless-steel clamp for connection to platinum wire (6). (7) Stainless-steel ring pressed onto tungsten potential probes.

by passing it through an isolation amplifier and was then fed to a digital electrometer. Measurements were made at temperature intervals of 20 to 50°C, at temperatures ranging from 20 to 550°C, and over several heating and cooling cycles. After changing the temperature, we waited a sufficient time (~1 hr) for thermal equilibrium conditions to reestablish before recording data. The total error in the measurements resulting from probe positioning and instrumentation was less than ±10%.

Photoelectron–Spectroscopic Measurements

Samples for the determination of the photoelectron spectra were prepared in a manner similar to those used to prepare samples for the conductivity measurements. After sintering, the disks were approximately 12 mm in diameter and 1 mm thick. The samples were transferred in an argon-filled container into a dry box attached to the sample chamber of the electron spectrometer. Before they were placed into the sample chamber, they were abraded lightly on Carbimet paper.

The spectra were determined with a GCA/McPherson ESCA36. In this instrument the electronic kinetic energies are measured with electrostatic plates consisting of spherical segments with a mean radius of 36 cm and a separation of 10 cm. The energy resolution is 0.02%. Mg $K\alpha$ X-rays were used for all the measurements. The window on the X-ray source is beryllium, and multichannel detection is used in our instrument. Hence scanning times used were approximately 5 min. The spectra were scanned over a 10-eV range with increments of 0.16 eV and 63 points. To correct for small electrical charges acquired by the samples, the binding energies were referred to the C(1*s*) binding energy (284.8 eV) of the carbonaceous contaminant on the samples. This procedure has been demonstrated to furnish reproducible results (*8*). The binding energies were determined by bisecting the curves in the vicinities of the maxima. The precision in the total procedure is approximately 0.05 eV.

Results and Discussion

Conductivity

X and copper-substituted X phases. The conductivity measurements were made on cylindrical samples of these phases between room temperature and 550°C. The results show that the X phase and the copper-substituted X phases are semiconductors with activation energies of 8–21 kJ $mole^{-1}$ (Table III). The conductivity of copper-substituted X phase, at the operational temperatures of the battery, is greater than that for X phase. An unusual behavior was observed around 225°C during the first heating cycle (Fig. 2). This behavior was nearly reproducible during successive heating and cooling cycles. At temperatures near 225°C, a change occurs in the character of the Arrhenius plots (Fig. 3). Above and below this temperature, the plots are linear with reproducible slopes. Near 225°C, the curves are somewhat nonrepro-

TABLE III

ACTIVATION ENERGY (E_a),[a] FOR VARIOUS HEATING AND COOLING CYCLES, FOR X AND Cu–X PHASES

Phase	E_a(kJ mole^{-1}) Low-temperature zone	E_a(kJ mole^{-1}) High-temperature zone
X		
Sample 1	20.3 ± 0.2	14.6 ± 0.2
Sample 2	20.3 ± 0.2	15.8 ± 0.2
Cu–X		
Sample 1	8.6 ± 0.2	9.0 ± 0.2
Sample 2	10.6 ± 0.2	11.4 ± 0.2

[a] Calculated from $\sigma = A \exp(-E_a/RT)$ relation.

ducible, but they have the general characteristic shown in Fig. 3. For the X phase, the activation energy for the high-temperature zone is lower than that of the low-temperature zone. The reverse of this appears to be true for the copper-substituted X phase. Precise characterizations of the plots of log σ vs T^{-1} are obscured somewhat by the fact that the data obtained during the cooling cycle do not reproduce as well as

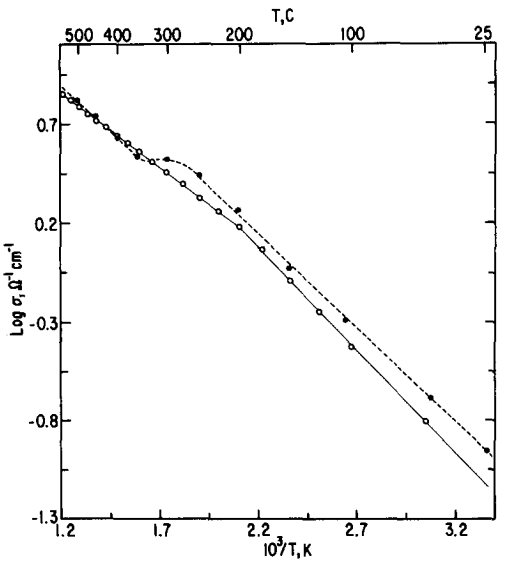

FIG. 2a. Arrhenius plot for X phase. First heating (●) and cooling (O) cycle.

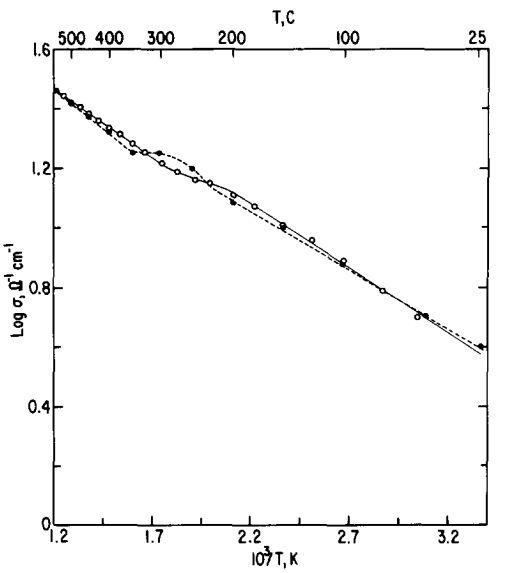

FIG. 2b. Arrhenius plot for Cu–X phase. First heating (●) and cooling (O) cycle.

one would expect. However, for the X phase the precision of the data obtained upon heating the samples is sufficient to reveal definitely a change in slope at 200°C. Thus a phase change occurs upon heating at this temperature. Although the measurements obtained during the cooling cycle demonstrate the change, in the region of the change the course of the plot is not sharp and reproducible. Thus we conclude that a phase change does occur but upon cooling it is somewhat sluggish. For the copper-substituted X phase, however, no well-defined phase change is indicated. In this case the small change which does possibly occur is sluggish in both cycles, if it does in fact occur.

J phase ($LiK_6Fe_{24}S_{26}Cl$). As mentioned earlier, our samples of this phase contained a significant amount of another phase as impurity, the composition of which could not be established. The room-temperature resistance of a cold-pressed disk of the mixture can be reported only within an order of magnitude; it was 2100 Ω at 25°C. When the pellet was heated, the conductivity in-

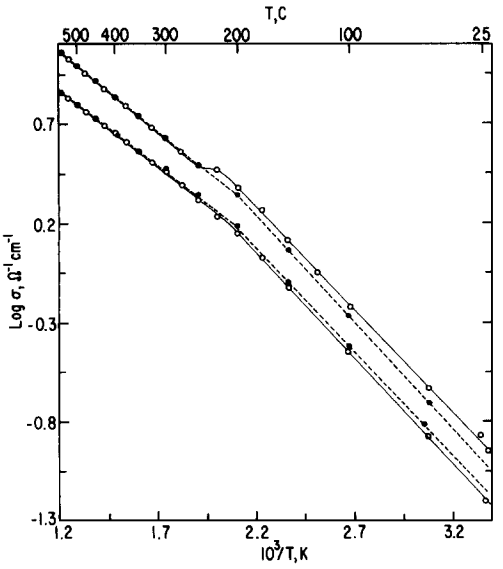

FIG. 3a. Arrhenius plots for X phase (two samples). Second heating (●) and cooling (○) cycle.

creased considerably at temperatures above 80°C, and the cooling cycle followed an entirely different path.

Z phase ($Li_3Fe_2S_4$). Measurements were made on two sintered disks of the Z phase

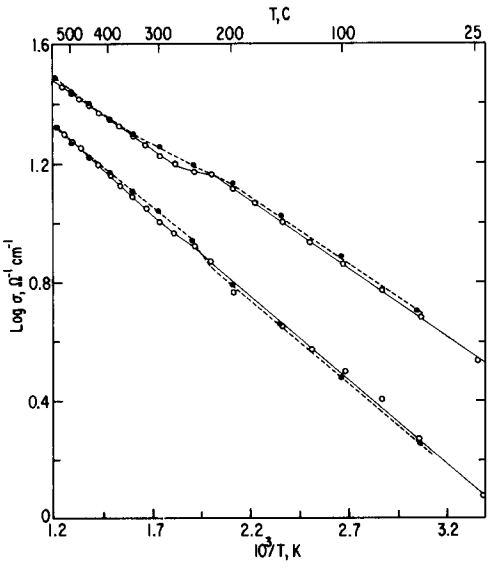

FIG. 3b. Arrhenius plots for Cu–X phase (two samples). Second heating (●) and cooling (○) cycle.

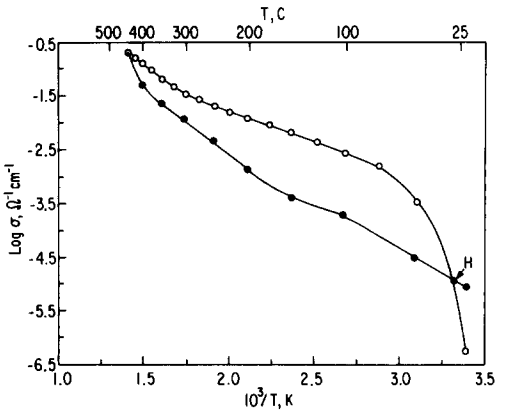

FIG. 4a. Arrhenius plot for Z phase, sample 1: (●) heating cycle, (○) cooling cycle.

between room temperature and 440°C. The data for one heating and cooling cycle for both samples are shown in Fig. 4. The conductivity of the Z phase is approximately three orders of magnitude lower than that of the X or the Cu–X phases at the cell operating temperatures. Moreover, the cooling cycle lies above the heating cycle. During the heating cycle no time-dependent behavior for conductivity was observed over the entire temperature range. Similar

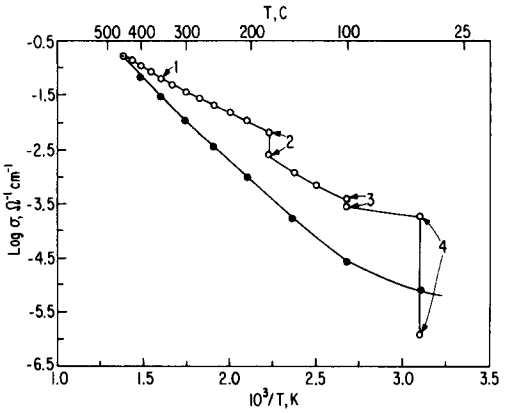

FIG. 4b. Arrhenius plot for Z phase, sample 2: (●) heating cycle, (○) cooling cycle. Numbers on the cooling curve indicate the change in the conductivity at a constant temperature over a period of time. Data points recorded at time intervals of: (1) 990 min at 374°C, (2) 930 min at 175°C, (3) 165 min at 160°C, and (4) 900 min at 50°C.

behavior was observed during the cooling cycle down to ~200°C. However, below this temperature, the conductivity became time dependent; the time dependence increased with decreasing temperature. This was confirmed by leaving the sample at 175°C for 15.5 hr. The change in conductivity was slow but over this time period conductivity decreased by a factor of ~2.3 (Fig. 4b). However, at 50°C the resistance of the sample increased by orders of magnitude. The results indicate that possibly a phase separation occurs during heating and cooling cycles. X-Ray diffraction patterns of the Z-phase sample used for the conductivity measurements showed the presence of only the Z phase. It is possible that phase separation occurs during heating and that Z phase is found again during cooling.

It is well known and recognized that the conductivity of polycrystalline samples is lower than that of single crystals. Contributions from grain boundaries (contact resistance and constriction of current lines) to the total resistivity can be significant if grains make poor contact. The sintering process increases grain size as well as interfacial contact between grains and thereby decreases grain boundary contributions. Activation energy of barrier layers at grain boundaries will be different if there is build up of a space charge layer. This could occur through partial blocking of charge carriers by precipitated impurities (less conducting phases) at grain boundaries. This has been recognized in solid electrolytes, e.g., in stabilized zircona-doped ceria and β alumina. For pure materials one suspects that the activation energies for polycrystalline material and for single crystals are nearly the same provided that the composition and electron density in the bulk and at the surfaces of the grains are the same.

Conductivity measurements were made on sintered pellets of X and copper-substituted X phases. The density of the X-phase disk was 2.38 g cm^{-3}; for copper-substituted X phase it was 2.98 g cm^{-3}. If 2.69 g cm^{-3} is taken as the theoretical density (*9*), then the X-phase disks used for conductivity measurements had a density which was 89% of the theoretical value. Metallographic examination showed both X and copper-substituted X phases to be reasonably pure. Although the absolute values of the conductivities are questionable, the activation energies should be comparable to those for single crystals.

Photoelectron Spectra

The spectra obtained from the photoelectron–spectroscopic measurements are displayed in Figs. 5 and 6. The binding energies derived from these spectra are listed in Table IV.

An examination of the binding energies for the S(2*p*) orbital electrons shows that the values are comparable in FeS, X phase, copper-substituted X phase, and Z phase. In all these cases, the binding energies are generally only 0.5 eV larger than that for S(2*p*) in Li_2S. This difference indicates that there occurs only a small change in the chemical environment of sulfur during the formation of these phases from FeS and Li_2S. The values for the binding energies for S(2*p*) in all these phases are less by ap-

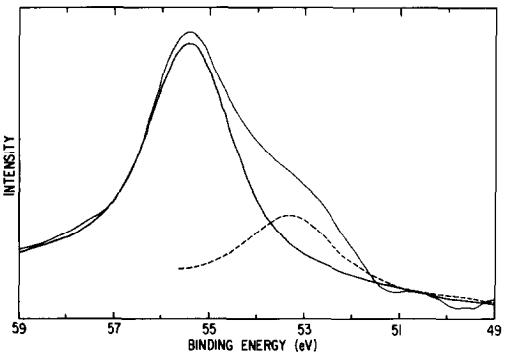

FIG. 5a. X-Ray photoelectron spectrum of Fe(3*p*) orbital electrons of Li_2FeS_2 (X phase). The same spectra were obtained for $Li_{1.33}Cu_{0.67}FeS_2$ (Cu-substituted X phase) and Z phase. Resolved shoulder attributed to Fe^{2+} is indicated.

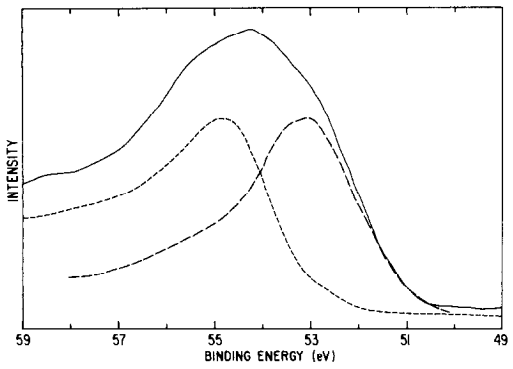

FIG. 5b. X-Ray photoelectron spectrum of Fe(3*d*) of $Li_{1.33}Cu_{0.67}FeS_2$ (Cu-substituted X phase) after bombardment with argon ions. Resolved shoulder attributed to Fe^{2+} has been increased by argon ion bombardment.

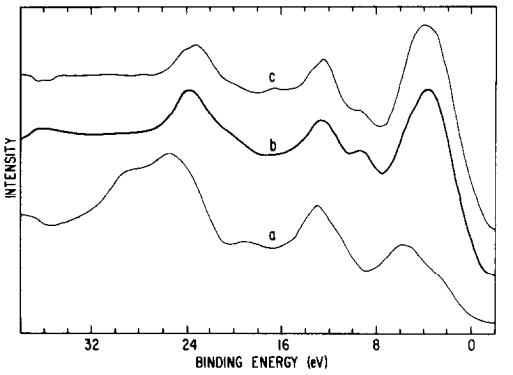

FIG. 6b. X-Ray photoelectron-spectroscopic spectrum of valence band of Li_2FeS_2 (X phase) before (a) and after (b,c) bombardment by argon ions.

proximately 1 eV than that in ZnS. Thus the sulfur in these phases is more negative than that in ZnS, probably because of the presence of free electrons in these phases. The value of S(2*p*) in the J phase is approximately 1.5 eV larger than in the other phases, probably because of the absence of free electrons and the presence of a more ionic environment.

The energy distribution curves for the Fe(3*p*) orbital electrons for the X phase, the copper-substituted X phase, and the Z phase all display shoulders on the low sides of the binding energies. Two possible sources exist for these shoulders: (1) the Li(1*s*) photoelectrons and (2) Fe(3*p*) photoelectrons from a lower valence state of iron. The first can be dismissed for two reasons. The fact that the binding energy for Li(1*s*) is at 54.6 eV and that the resolved maximum causing the shoulder is at 53.2 eV indicates that the shoulder cannot be attributed to the Li(1*s*) photoelectrons. In addition, an examination of the intensities indicates that the contribution of the Li(1*s*) photoelectrons is significantly less than the intensity contributed by the resolved maximum. Through a comparison of the intensities of S(2*p*) orbital electrons in Li_2S and in the copper-substituted X phase one can estimate that the contribution of Li(1*s*) photoelectrons to the energy distribution curve for copper-substituted X phase should be 7

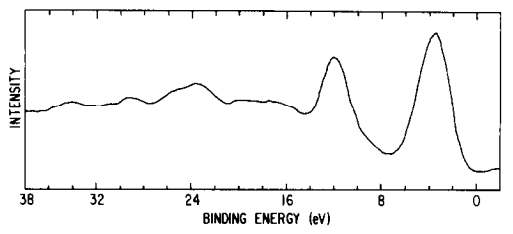

FIG. 6a. X-Ray photoelectron spectrum of valence band of Li_2S.

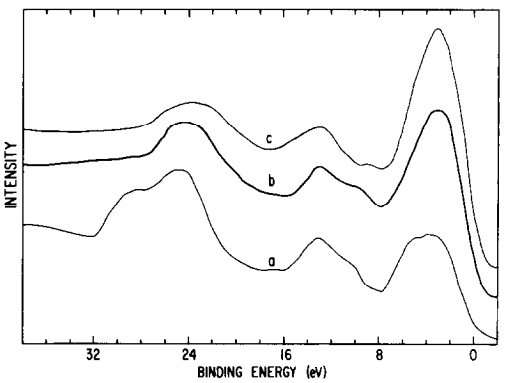

FIG. 6c. X-Ray photoelectron–spectroscopic spectrum of valence band of $Li_{1.33}Cu_{0.67}FeS_2$ before (a) and after (b,c) bombardment by argon ions.

TABLE IV

BINDING ENERGIES OF Li–Fe–S PHASES DERIVED FROM PHOTOELECTRON SPECTROSCOPY

Phase	"Formal valence" of Fe	Binding energies (eV)				
		S(2p)	Fe(3p)		Fe(3d)	Fe(3p)–Fe(3d)
Fe			52.42		0.58	51.84
FeS	2+	160.7[a]	52.4[a]	53.0	3.7	
		161.6[b]	53.5[b]			
Cu–X	2+	160.85	55.16	53.1	3.62	51.54
X	2+	160.89	55.29		5.52	49.77
Z	2.4+	160.73	54.91			
J	2+	162.45	55.88		7.6	48.28
FeS_2		162.82	54.14		1.29	52.85
ZnS		161.92				
FeF_2	2+		56.21			
Li_2S		160.41	(54.59)[c]		(3.5)[d]	

[a] Data drawn from Kramer and Klein.
[b] Data drawn from Gopalakrishnan *et al.* (*11*).
[c] Li(1s).
[d] S(3p).

c/s. Since the intensity of the Fe(3p) peak is 58 c/s and since that for the resolved shoulder is 18 c/s, it seems unlikely that the Li(1s) photoelectrons make a sufficiently significant contribution to the energy distribution curve. Consequently, we eliminate the Li(1s) photoelectrons as the source for the shoulder and assign it to a lower valence state of iron. Thus X, copper-substituted X, and Z phases all contain iron in two valence states, assumed to be Fe^{3+} and Fe^{2+}. Upon bombardment with argon ions the ratio of the Fe^{2+} to Fe^{3+} increases in the copper-substituted X phase. Since the argon ion bombardment not only removes surface contaminants, such as oxides, but also can produce some reduction of the material, one cannot derive a reliable measure of the two valence states; however, we estimate that the actual ratio of the two valence states is intermediate between those indicated in Figs. 5b and c.

The spectra in the vicinity of the valence bands are shown in Figs. 6a, b, and c. In general the structures of the spectra consist of two maxima which can be interpreted in terms of the spectra for Li_2S (Fig. 5a) and FeS (*10, 11*). In the first case, the two maxima at 3.5 and 12.0 eV can be assigned to the photoemission of electrons from the S(3p) orbital and S(3s) orbitals, respectively. In the published spectrum for FeS valence band (*10, 11*) the energy distribution curve consists of a broad maximum with several shoulders on both sides. The broad maximum is at 3.7 eV. Thus the S(3p) and Fe(3d) curves overlap extensively. The envelope for Fe(3d) is broadened by the multiplicity of final states which are possible for the $3d^5$ configuration. It is also made more complex by the fact that the iron ion, whether Fe^{3+} or a mixture of Fe^{3+} and Fe^{2+}, is not in its ground state initially (*12*). Thus the valence band in FeS consists of a composite of a large number of states. At the zero of the energy scale, i.e., at the Fermi level of the electron spectrometer, the curve for Li_2S is essentially zero. That for FeS, however, is significantly different from zero. Thus the essential difference between the insulating Li_2S and the conducting FeS is not a difference in the energies at

the maxima but a difference in the width and, consequently, the fact that the valence band is essentially zero at the Fermi level for Li_2S but it has a significant value at the Fermi level for FeS.

The valence band spectra for X and copper-substituted X phases displayed in Figs. 6b and c show the enhancement of the first maxima relative to those for S(2*s*) photoemission upon bombardment of the phases with argon ions. For the most part, this enhancement is accomplished by an increase in the lower valence state for iron as shown in the spectrum for Fe(3*p*) for the copper-substituted X phase (see Fig. 5c). Since the bombardment with argon ions tends to reduce the iron, as cited above, the actual situation existing in the valence band is somewhat intermediate between that represented by the spectrum for the unbombarded case and that for the first bombardment. Fortunately, whatever the extent of the reduction, the structure does not change significantly. In the case of the X phase, the valence band is composed of the S(3*p*) and the Fe(3*d*) densities. In the case of the copper-substituted X phase, the Cu(3*d*) density is also contained in the envelope. The Fe(3*d*) and Cu(3*d*) densities also contain components from the final states and from the crystal field splittings of the initial states. Because the S(3*p*) and the 3*d* densities overlap so extensively, the net energy associated with charge exchange between cations and anions is small. However, there exist barriers at the saddle points, so that the activation energies for charge exchange are larger than the net energies. In any event, the conductivities involve a complexity of processes consisting of charge exchanges between cations and anions for the *p* type and nonzero densities at the Fermi levels for the *n* type. In a broad sense, however, one recognizes that the energies at the maxima, and hence the densities at the Fermi level, are in the same order as are the conductivities.

All the phases cited above and some others cited below can be understood structurally, stoichiometrically, and electrochemically as derivatives of FeS. There occur several forms of FeS or phases with stoichiometry near FeS, but essentially the structure in the NiAs structure or a distorted NiAs structure. This structure has a hexagonal unit cell with 12 molecules per unit cell. Wyckoff places the atoms to correspond to the D_{3h} space group. In this arrangement the atoms are in the same positions of C_{6v} that are occupied in graphite, but the axial ratios and values of *u* are so different that the atomic groupings are not similar. In any event, the structure tends to be a layered one, and the electrical properties are anisotropic. The lithium ions undoubtedly diffuse in readily and may be located randomly, a surmise which is consistent with the fact that their positions cannot be detected by neutron diffraction.

If these phases were insulators, the stoichiometry would require that the sulfur valence is 2− and that for the iron is 2+. Because the value for S(2*p*) binding energy is nearly that for S^{2-}, it seems plausible to assume that such is in fact its valence. The photoelectron spectroscopic spectra for Fe(3*p*), however, indicate that the iron is in both the 2+ and 3+ state, a fact which is consistent with free electrons in X, copper-substituted X, and Z phases. This description is consistent with the properties of the lanthanide monosulfides in which the occurrence of insulators or conductors is rationalized in terms of S^{2-} and 2+ or 3+, respectively, for the metal. For consistency then, one would expect FeS to contain both 2+ and 3+ states. However, no evidence for such has been found (*11*).

In addition to the phases which were studied herein, there are several other phases in the Li–Fe–S system which were identified. All of them are listed in Table V in order of increasing ratio of lithium to sulfur. Also listed in this table are the binary

TABLE V

PHASES OBSERVED IN THE Li–Fe–S SYSTEM

Empirical formula	Binary composition	Lithium-to-sulfur ratio	Reference
$Li_2Fe_2S_4$	$Li_2S \cdot Fe_2S_3$	0.50	(*2*)
$Li_4Fe_3S_6$	$2Li_2S \cdot Fe_3S_4$	0.67	(*1*)
$Li_3Fe_2S_4$(Z)	$3Li_2S \cdot Fe_4S_5$	0.75	(*13*)
Li_2FeS_2(X)	$Li_2S \cdot FeS$	1.00	(*1, 3, 4*)
$Li_{12}Fe_4S_{11}$(W)	$6Li_2S \cdot Fe_4S_5$	1.09	(*13*)
$Li_7Fe_2S_6$(Y)	$7Li_2S \cdot Fe_4S_5$	1.17	(*13*)

compositions: Li_2S and $Fe_{1-x}S$. An examination of the stoichiometries reveals that the first phase listed, $Li_2Fe_2S_4$, should be an insulator. All the others are semiconductors.

The electrochemical process involved at the FeS cathode of the LiCl–KCl–FeS cell is one in which the lithium ion migrates from the electrolyte into the FeS and displaces the Fe ion. The migration is ambipolar so that electrons must accompany the lithium ion. The reaction is

$$2FeS + 2Li^+ + 2e \rightarrow Li_2FeS_2 + Fe.$$

The resultant chemical potential is not so much that directly associated with the lithium ion, but rather that associated with the change which occurs in the chemical potential of the free electrons. And the process is reversed by the ambipolar migration of the lithium ion as a result of the flux of electrons.

Acknowledgments

We express our thanks for useful discussions with J. Battles, D. Vissers, and R. K. Steunenberg; we thank K. Jensen for the chemical analysis and J. Battles for the metallographic examination of the samples; and we express our thanks to Brenda Grazis for typing the manuscript and to Elsie M. Klasek for preparing the figures.

References

1. R. A. SHARMA, *J. Electrochem. Soc.* **123,** 448 (1976).
2. C. A. TAFT, S. F. DACUNHA, N. G. DESOUZA, AND H. C. FURTADO, *J. Phys. Chem. Solids* **41,** 61 (1980).
3. P. A. NELSON AND D. S. WEBSTER, ANL 8084, Argonne National Laboratory, Argonne, Ill., April 1974.
4. A. E. MARTIN, R. K. STEUNENBERG, AND Z. TOMCZUK, Paper 54 at The Electrochemical Society Meeting, New York, October 13–17, 1974.
5. Argonne National Laboratory Reports ANL 78–94, November 1978, and ANL 79–39, May 1979.
6. B. S. TANI, *Zmer. Mineral.* **62,** 819 (1977).
7. C. A. MELANDRES AND B. TANI, *J. Phys. Chem.* **82,** 2850 (1978).
8. G. E. MURCH AND R. J. THORN, *J. Phys. Chem. Solids* **41,** 785 (1980).
9. S. SIEGEL, Chemical Engineering Division, Argonne National Laboratory, private communication.
10. L. N. KRAMER AND M. P. KLEIN, *J. Chem. Phys.* **51,** 3618 (1969).
11. J. GOPALAKRISHNAN, T. MURUGESON, M. H. HEDGE, AND C. N. R. RAU, *J. Phys. C* **12,** 5255 (1979).
12. R. J. THORN, *J. Phys. Chem. Solids,* **43,** 393 (1982).
13. J. BTTLES AND D. VISSERS, Chemical Engineering Division, Argonne National Laboratory, private communication.